



## Rock mass response ahead of an advancing face in faulted shale

Salina Yong<sup>a,\*</sup>, Peter K. Kaiser<sup>b</sup>, Simon Loew<sup>a</sup>

<sup>a</sup> Department of Earth Sciences, ETH Zurich, Sonneggstrasse 5, 8092 Zurich, Switzerland

<sup>b</sup> Centre for Excellence in Mining Innovation, 935 Ramsey Lake Road, Sudbury, Ontario, Canada P3E 2C6

### ARTICLE INFO

#### Article history:

Received 15 March 2012

Received in revised form

22 November 2012

Accepted 2 January 2013

#### Keywords:

Tunnelling

Nuclear waste disposal

EDZ

Opalinus clay

### ABSTRACT

In this study, the rock mass response ahead of an advancing test tunnel in the Opalinus Clay at the Mont Terri Rock Laboratory (Switzerland) was investigated. Characterisation of the excavation-induced damage zone at Mont Terri is a challenging task due to the anisotropic and heterogeneous nature of the shale: pronounced bedding leads to intact rock anisotropy and prevalent small-scale tectonic shears lead to rock mass heterogeneity. Rock mass damage ahead of an experimental tunnel or niche was characterised through single-hole seismic wave velocity logging, borehole digital optical televiewer imaging, and geological drillcore mapping. Three-dimensional elastic stress analyses were completed and showed that rock mass degradation can be correlated to changes in the maximum to minimum principal stress ratio (i.e., spalling limit). Numerical results showed that close to the niche boundary, unloading lowers stress ratios, which correspond with decreasing seismic wave amplitudes and velocities; thus, indicating that strength degradation resulted from increasing crack-induced damage. Considerations of tectonic shears and distance from a previously stressed volume of rock were necessary in understanding both the damage state and extent ahead of the face. By integrating field and numerical data, the investigation showed that geological structures (i.e., bedding and bedding-parallel tectonic shears) were most influential near the entrance but played a lesser role as the niche deepened. Additionally, a portion of the niche is located in the perturbed zone of the intersecting Gallery04.

© 2013 Elsevier Ltd. All rights reserved.

### 1. Introduction

Tunnel construction damages the surrounding rock mass, which can lead to the alteration of rock mass transport properties and/or tunnel instability. Safety assessment of geological nuclear waste repositories necessitates understanding the processes that lead to rock mass perturbations induced by tunnel excavation. While many previous studies have investigated perturbations around tunnels in shale, few have considered the development of perturbations ahead of an advancing tunnel. However, degradation of the rock mass ahead of the advancing face may influence development of the perturbed zone around the tunnel away from the face: e.g., possibly leading to asymmetric tunnel breakouts [1].

Abel and Lee [2] demonstrated that changes in the stress state can be detected several tunnel diameters ahead of the face in both laboratory and field studies. The laboratory studies involved tunnelling in models built from acrylic (ideally elastic), concrete (heterogeneous elastic), and granite (approximately elastic brittle). The onset of stress changes were detected two to four diameters

ahead of tunnels drilled into the laboratory models. Compressive stress peaks, one to two diameters ahead of the tunnel, were also measured in these models. In the field study, two probes were installed about 15 m ahead of a proposed crosscut in jointed and closely foliated gneiss and gneissic granite. Changes in stress associated with the advancing tunnel were measured more than seven tunnel diameters ahead of the face with a compressive stress peak about six tunnel diameters away from the advancing face. This was followed by a much larger decrease in compressive stress. Stress-change trajectories were also determined from the field measurements and demonstrated that local structural variations in the foliated and faulted metamorphic rocks controlled the rock mass response. The crosscut was driven orthogonal to the strike of the major geological weakness in the rock mass, or the foliation in this case. Because the foliation and associated jointing provided a ready avenue for tensile strain relief, the rock mass was postulated to have expanded preferentially perpendicular to the foliation and towards the advancing face. In this case, strain relief was provided parallel with the crosscut axis and normal to the strike of foliation. Overall, the tunnel advance resulted in decompression of the rock mass ahead of the face and to the side of the tunnel.

Read et al. [1] and Martin [3] investigated the development of v-shaped notches around a test tunnel that was excavated in the Lac du Bonnet granite, and concluded that notch development

\* Corresponding author. Present address: MIRARCO, 935 Ramsey Lake Road, Sudbury, Ontario, Canada P3E 2C6. Tel.: +1 7056751151x5097; fax: +1 7056754838. E-mail address: syong@mirarco.org (S. Yong).

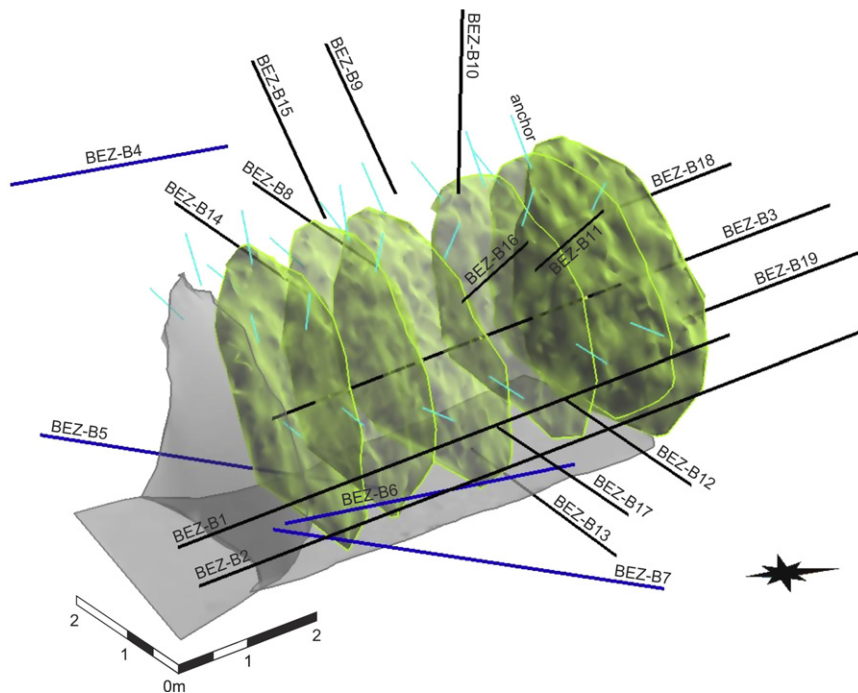


Fig. 1. Isometric view of the various EZ-B niche faces, boreholes, and roof anchors.

depended on changes in the stress state ahead of the face. The Mine-by Experiment tunnel was aligned roughly with the intermediate principal stress ( $\sigma_2$ ) axis while the minimum principal stress ( $\sigma_3$ ) axis was sub-vertical. The maximum principal stress ( $\sigma_1$ ) was nearly orthogonal to the tunnel axis. V-shaped notches formed in the roof and floor of the tunnel about 0.6 m behind the face. The notches were not diametrically opposed due to non-symmetric stress concentrations caused by a  $10^\circ$  offset of the tunnel axis with the intermediate principal stress direction [1]. Stress path analyses indicated that well ahead of the advancing face in regions where the notches formed, the crack initiation threshold [4] was exceeded and thus, damage was in the form of micro-fracturing. Additionally, principal stress rotations, when stress levels exceeded crack initiation, also initiated ahead of the face with the maximum rotation in  $\sigma_3$  occurring in the roof. Consequently, rock mass degradation near the tunnel perimeter may be further exacerbated. Through a numerical study, Eberhardt [5] found magnitude and directional changes in the redistributed stress field near the face differed depending on the tunnel alignment with the far-field principal stress axes. It was postulated that magnitude and directional changes in the redistributed stress field would lead to progressive accumulation of damage.

Investigations relating to nuclear waste storage in argillaceous media have also shown rock mass perturbations initiating ahead of the face. Induced fracturing has been mapped in tunnel faces at the Meuse/Haute-Marne Underground Research Laboratory in France [6] and at the HADES Underground Research Facility in Belgium [7]. In both cases, fracturing formed an open “v” with a horizontal axis of symmetry near the tunnel springline. Fracturing was also found to be more pronounced when the tunnel axis was aligned parallel with the maximum horizontal stress at Meuse/Haute-Marne.

The Opalinus Clay in Switzerland is under consideration as a potential host rock for the storage of nuclear waste [8]. At the Mont Terri Rock Laboratory, the typical zone of perturbation around the tunnel cross-section consists of sub-vertical extension fracturing in the sidewalls and bedding-parallel fracturing above

the crown and below the invert [8]. The rock mass response several metres ahead of the face has been examined in the EDB section of Gallery98 [9], HG-A niche in Gallery04 [10], and the MB section of Gallery08 (unpublished reports are currently under review, CD Martin, pers. comm.). This paper examines the rock mass response immediately ahead of an advancing face before and during the excavation of a short test tunnel, the EZ-B niche (Fig. 1), at the Mont Terri research facility.

## 2. The Mont Terri Rock Laboratory

The EZ-B niche is located in Gallery04 (Fig. 2) at the Mont Terri Rock Laboratory in northern Switzerland. Mont Terri is the northernmost in a series of anticlines in the Jura Mountains and the research facility is located in the southern limb, which is weakly deformed and less tectonically disturbed [11]. The anticline was formed by fault-bend and fault-propagation folding [12]. At the laboratory scale, tectonic features consist of networks of thin (i.e., in the order of millimetres) shear zones and a larger thrust fault zone [11,12].

Three sets of tectonic shears have been mapped in Gallery04 [12] but only two intersect the EZ-B niche [13]. The most frequently occurring is sub-parallel with bedding and dips south-southeast. On average, the bedding-parallel shears in the niche dip  $46^\circ$  towards an azimuth of  $146^\circ$  [13], resulting in a strike that is roughly perpendicular to the niche axis (Fig. 2). The bedding-parallel shears are closed and sealed with calcite and clay minerals. The second set are minor sub-horizontal shears that dip south to southwest and are found in isolated regions in the niche [13]. The sub-horizontal shears dip from  $0^\circ$  to  $20^\circ$  towards azimuths of  $132^\circ$  to  $186^\circ$  [13]. In the niche, sub-horizontal shears are bound by the bedding-parallel shears. Surfaces of both sets are slickensided and indicate thrusting towards the northwest [12].

The in situ stress field (Fig. 2) consists of sub-vertical maximum ( $\sigma_1$ ) inclined towards the south-southwest and sub-horizontal minimum ( $\sigma_3$ ) inclined towards the northeast

[14,15]. The intermediate principal stress ( $\sigma_2$ ) is sub-parallel with the axis of the EZ-B niche (offset of roughly  $14^\circ$ ).

The Opalinus Clay is shallow marine, dark grey Jurassic shale consisting of claystone and marl with intercalated sandy and calcareous layers and lenses. At Mont Terri, the formation consists of three facies. The niche is in the shaly facies, where bedding is millimetres thick with an average dip angle of  $45^\circ$  and dip direction of  $147^\circ$  [13]. The niche trends sub-perpendicular to the strike of bedding (Fig. 2).

### 3. The EZ-B niche

The EZ-B niche has a diameter of 3.8 m and length of 6–7 m (Fig. 2). Construction of the niche and associated borehole drilling campaigns spanned a period of 5 months from December 2004 to April 2005. In December, an entrance to the niche with a length of 1–2 m was excavated. The rock surface was lined with 150-millimetre-thick fibre-reinforced shotcrete and a 300-millimetre-thick concrete floor slab. Three 100-millimetre-diameter horizontal observation boreholes (BEZ-B1 to B3) with lengths of 8–9.5 m were drilled in February 2005. The remaining “main body” of the niche (Fig. 2) was excavated over a 12-day period in March 2005. Excavation of the niche was completed with a pneumatic hammer except for the entrance, where a roadheader was also used [13]. Due to the advantageous orientation of the niche axis with the bedding-parallel shears and bedding, minimal support was required. Roof support consisted of a steel mesh, aluminium nails, and 25-millimetre-diameter steel anchors. The anchors were grouted with a nominal embedment length of 0.5 m but were not tensioned.

Construction of the niche involved three stages [16]: pre-, syn-, and post-excitation of the main body of the EZ-B niche (Fig. 2). The pre-excitation stage (from December 2004 to February 2005) involved the entrance excavation and drilling of the first three boreholes, BEZ-B1 to B3. Excavation of the remaining 5.1 m of the main body occurred in the syn-excitation stage (March 2005). In Syn1, the first 65 cm was excavated in 2 days. One metre was excavated in the second round (Syn2), which was completed

2 days after Syn1. Syn3 resulted in an advance of 85 cm. The largest round of roughly 1.3 m was excavated in Syn4 and involved a wedge failure that occurred in the upper half of the advancing face. Syn5 entailed 90 cm of advance and 40 cm in Syn6. Syn3 to Syn6 were completed consecutively with a 12-hour stoppage between each round. The post-excitation stage started in April 2005 and consisted of the drilling of an additional 12 boreholes, BEZ-B8 to B19 (Fig. 1).

### 4. Data integration

The rock mass response ahead of the advancing niche face was evaluated by integrating data collected from the central borehole, BEZ-B3 (Figs. 1 and 3), as it was shortened to its final length of roughly 3 m. Borehole field data included drillcore mapping, digital optical televiewer (DOPTV) imaging, and single-hole seismic wave measurements. Other field data included laser scans and geological mapping of the niche surfaces. Numerical data from elastic continuum simulations were also incorporated.

The excavation geometry (niche boundary at each excavation step), location of borehole collars (Fig. 1), and location of tectonic shears (Fig. 4) were delineated from point clouds acquired by a panoramic laser scanner and corroborated against geological maps [17]. The dip and dip direction of the 12 intersecting tectonic shears were also determined from the laser scans and validated with measurements made during geological mapping of the niche and Gallery04 excavations (Fig. 4). Locations of the shears were also checked against those mapped in drillcores (Fig. 3) and found to be in general agreement.

Single-hole seismic wave measurements were acquired with the BGR (German Federal Institute for Geosciences and Natural Resources) mini sonic probe, which consists of four piezo-electric transducers: one source and three receivers at 10-centimetre spacing [18]. The larger the separation between the source and receiver, the greater the depth of seismic wave penetration. For the BGR mini-sonic probe, a penetration depth of 1–2 cm has been determined from finite difference modelling (K Schuster, pers. comm.). Hence, channel 1 is most affected by drilling related damage whereas

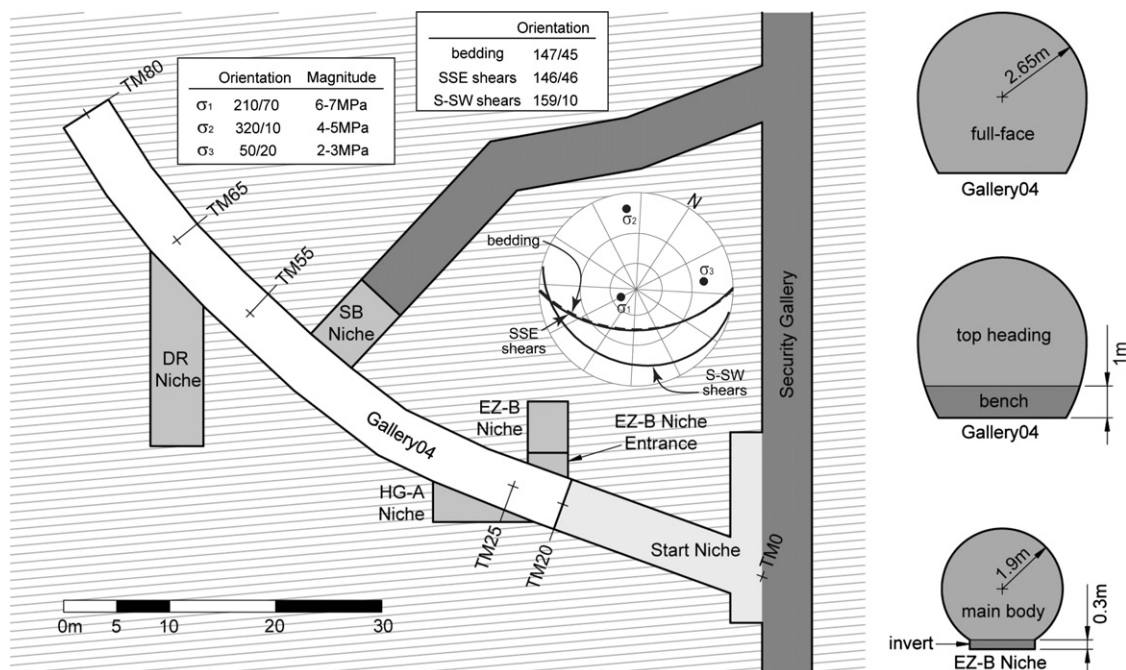
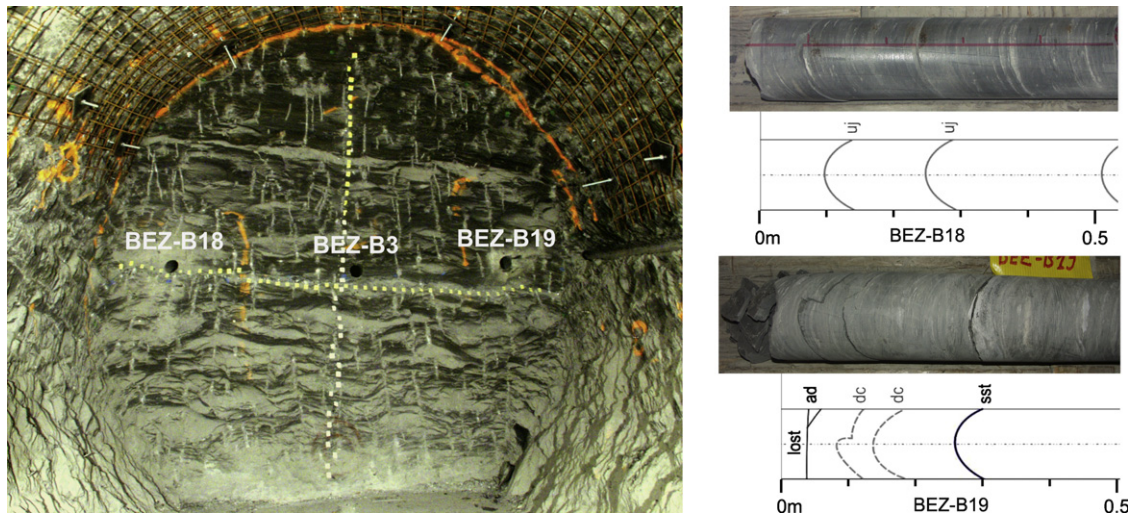
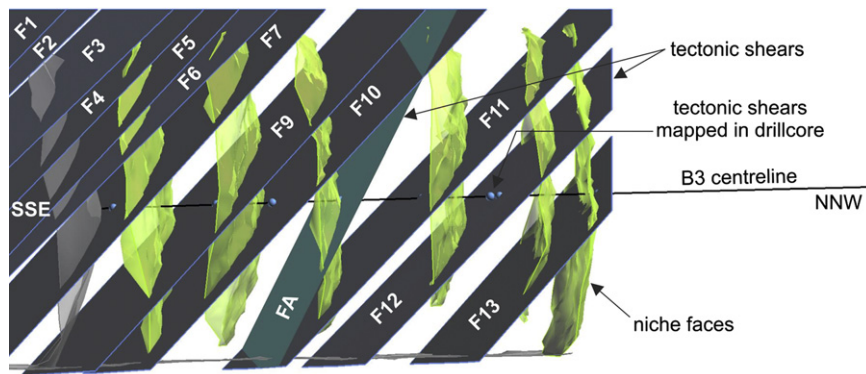


Fig. 2. The Mont Terri Rock Laboratory around the EZ-B niche in 2004 with lower hemisphere projections of the situ stress field and relevant geological structures (insets).



**Fig. 3.** Boreholes drilled into the final EZ-B niche face. Structures mapped in drillcore include: artificial discontinuities (ad), desiccation cracks (dc), unloading joints (uj), and tectonic shears (sst).



**Fig. 4.** Tectonic structures mapped in the EZ-B niche. FA is a potential steeper-dipping shear between Syn3 and Syn4 faces.

channel 3 is least affected. P-wave (compression) and S-wave (shear) velocities and respective amplitudes were derived from first-arrival phases as the probe moved at intervals of 5–10 cm.

To understand the changes in stress within the surrounding rock mass, numerical modelling was carried out with FLAC3D (Fast Lagrangian Analysis of Continua in Three Dimensions), version 3.00–308 [19]. Two identical elastic continuum models were simulated. The volume of rock modelled (Fig. 5) was 65 m in width, 77 m in length, and 65 m in height (i.e., five to eight tunnel diameters). External boundaries were fixed in all three directions and the initial stress state consisted of that shown in Fig. 2. The excavation of three openings was simulated starting with Gallery04 followed by the HG-A and EZ-B niches. Gallery04 was simplified as a straight line (69 m long) and excavated full-face in 33 steps, which approximated the as-built advance [12]. As per the as-built sequence, the HG-A niche excavation was simulated in three steps with the last step including the entrance of the EZ-B niche: these excavation activities are those completed in the pre-excavation stage. Finally, the EZ-B niche was excavated in seven steps with the main body excavated in the first six steps (Fig. 1) and the invert in the seventh step. Two sets of material properties [20,21] were considered (Table 1). Elastic isotropic (CIE) properties were implemented in the first set while the second set consisted of a transverse isotropic matrix (CAE) with the plane of transverse isotropy dipping 45° towards 147°.

Field and simulated borehole data from each excavation round were integrated as shown in Fig. 6. The data plotted in Fig. 6 was collected in borehole BEZ-B3 (Fig. 1) during the pre-excavation

stage, which serves as a benchmark for interpreting the perturbations induced ahead of the niche face. The position of the advancing face and intersecting bedding-parallel shears are shown in the top image. Blue spheres coincide with bedding-parallel shears that were mapped in the drillcore. Principal maximum and minimum stress ratios along the centreline of the borehole were extracted from the numerical simulations and are plotted below. Channel 3 S-wave velocities ( $V_s$ ) and associated normalised amplitudes ( $NA_s$ ) follow. Only Channel 3 data is considered for deriving S-wave parameters as it is the least affected by borehole drilling [18]. P-wave velocities ( $V_p$ ) and corresponding normalised amplitudes ( $NA_p$ ) from all three channels are plotted below the S-wave data. Normalisation of the seismic wave amplitudes was necessary to enable comparison between the channels as attenuation increased rapidly with increasing distance between the source and receiver. Both amplitudes were normalised by the average of each respective channel [18]. The corresponding drillcore map and unwrapped DOPTV image are provided at the bottom of the figure. The DOPTV image has been rotated such that the horizontal centreline of the image coincides with the travel path of the mini-sonic probe. In the case of BEZ-B3, the travel path of the probe was along the east borehole wall.

## 5. Damage observations

In the pre-excavation stage, 38 fractures were mapped in the BEZ-B3 drillcore. None of the fractures were identified as excavation-induced fractures (or “unloading joints”). Five bedding-parallel shears

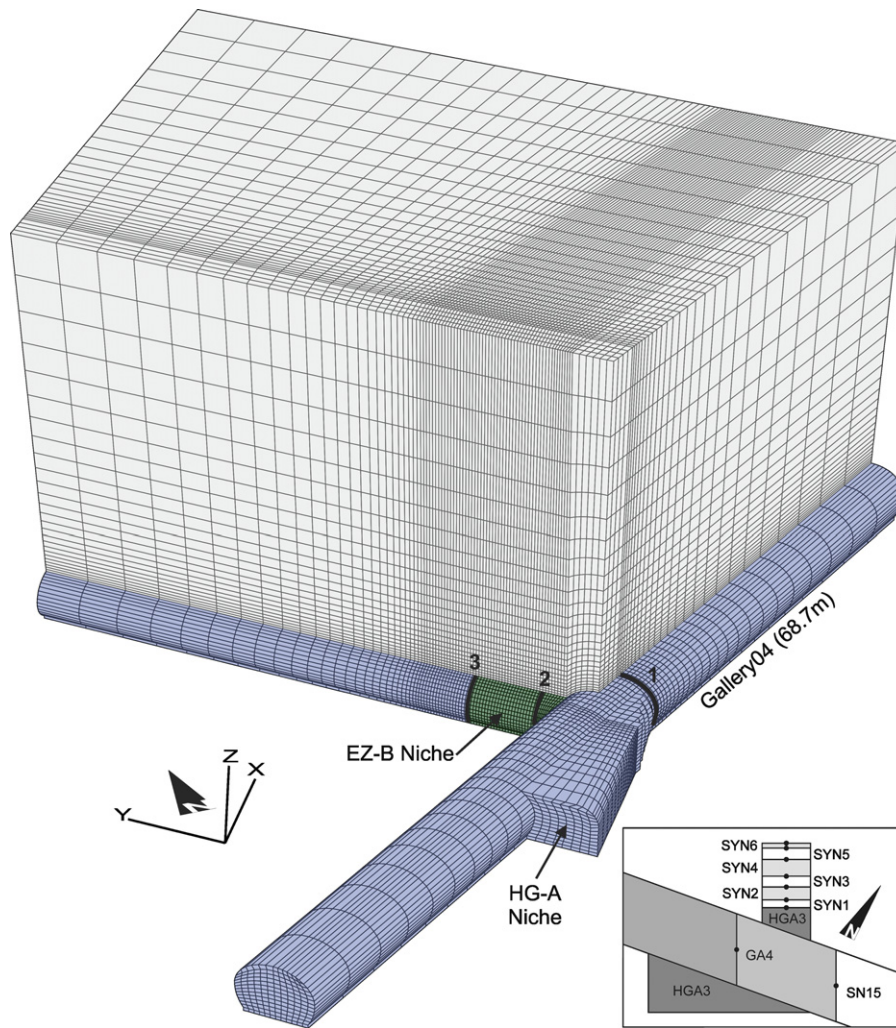


Fig. 5. Excavations simulated in the continuum analyses (looking northeast) with excavation steps labelled in the inset.

**Table 1**  
Material properties used in the elastic anisotropic continuum model [17,18].

	Isotropic (CIE)	Anisotropic (CAE)
$E$ (bedding parallel)	6–7 GPa	10 GPa
$E$ (bedding perpendicular)		4 GPa
$G$ (bedding perpendicular)	1.2–3.5 GPa	1.2–3.5 GPa
$\nu$ (bedding parallel)	0.27–0.29	0.33–0.35
$\nu$ (bedding perpendicular)		0.24–0.25

were mapped while the remainder were identified as “artificial discontinuities” [13]. The lack of “unloading joints” is not surprising as excavation of the entrance removed the first one to two metres of rock mass where the induced macroscopic fracture frequency would be at its highest. However, the persistent and pervasive nature of the bedding in the Opalinus Clay makes it challenging to map drillcore at Mont Terri. For example, 77% of BEZ-B3 drillcore fractures are parallel with bedding and six “artificial discontinuities” were mapped where bedding-parallel shears were projected to intersect the niche (Fig. 6). Artificial discontinuities are attributed to drillcore extraction and handling. Despite the small number of macroscopic fractures mapped in the drillcore, perturbations are evident in the seismic wave data (Fig. 6) where both seismic wave velocities and normalised amplitudes are lowest in the first 1.1 to 1.6 m ( $V_p$  and  $NA_p$ , respectively). Closer examination of the seismic wave data also shows

that velocity and amplitude lows locally coincide with intersections of bedding-parallel shear (arrows in Fig. 6). This data appears to indicate that the benchmark damage of BEZ-B3 is more microscopic in scale.

In the syn-excavation stage, the DOPTV images were used to identify induced macroscopic fractures [17]. However, it quickly became evident that this method requires significant fracture aperture. Furthermore, BEZ-B3 was uncased, uncovered, and the niche humidity was not controlled (these factors are especially critical in argillaceous media), which in turn intensified reliance on the seismic wave data for assessing damage ahead of the niche face.

Seismic wave data from each repeat borehole logging, along with the benchmark from the pre-excavation stage (Fig. 6), are compiled in Fig. 7. A profile view of the niche is shown at the top of Fig. 7: the entrance face is shown in light grey, the six syn-excavation faces are shown in yellow, intersecting tectonic shears are shown as dark grey planes, the centreline of borehole BEZ-B3 that runs nearly central to the niche body is shown as a black line, and the tectonic shears mapped in the drillcore of BEZ-B3 are shown as blue balls. It should be noted that the balls coincide well with the projected planes of the tectonic shears that were located from the laser scans. The series of plots below the niche image are of the seismic parameters derived from the single-hole seismic wave measurements: the velocity ( $V_p$  for P-wave and  $V_s$  for S-wave) and corresponding normalised amplitude (NA) profiles from each of the three channels (“1” is closest to and “3” is

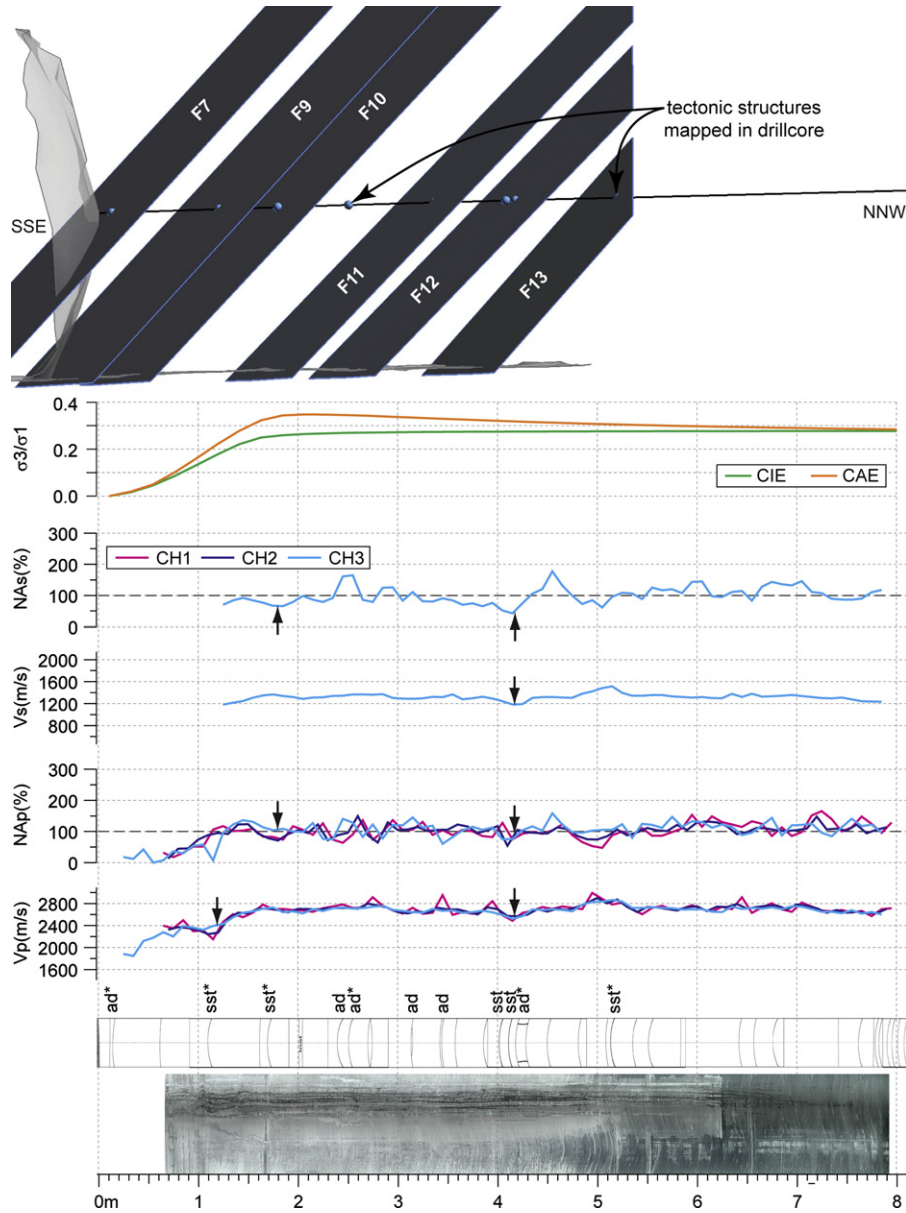


Fig. 6. Integration of pre-excitation BEZ-B3 borehole data. Asterisks indicate drillcore structures mapped closest to projected intersections of bedding-parallel shears.

farthest away from the source). The black line represents the benchmark measurement, which was made after excavations of the EZ-B niche entrance and the nearby HG-A niche (pre-excitation stage). The remaining “SYN” lines represent repeat measurements made after each niche excavation step. The number following “SYN” coincides with the respective niche excavation step, as shown in the inset of Fig. 5.

The extent of the perturbed zone (Fig. 8) ahead of the advancing niche face is then determined by comparing the repeat seismic wave measurements with the benchmark established in the pre-excitation stage for all three channels. It is important to note that damage associated with borehole drilling has the greatest effect on channel 1 wave propagation but diminishes with distance from the source: Channel 3 wave propagation is thereby least affected by damage associated with borehole drilling. Nonetheless, reductions in both velocities and normalised amplitudes can be discerned in the channel 3 data plotted in Fig. 7, similar to those of channels 1 and 2. From this comparison against the benchmark levels, it can be seen that the lowest seismic wave velocities and amplitudes are consistently found immediately ahead of the advancing face or

within about 0.3–1.5 m from the various advancing faces (yellow surfaces at the top of Fig. 7).

As an aside and in response to a commonly asked question, an attempt was made to correlate the excavation advance with the extents of perturbation (Fig. 8) but this proved unsuccessful. As shown in Fig. 8, the smallest and largest advances (i.e., Syn6 and Syn4, respectively) resulted in similar extents of roughly 1 m. Similarly, the smallest and largest zones of perturbation, measuring respectively 0.3 m in Syn3 and 1.2 m in Syn5, corresponded with similar excavation advances of 0.85 m in Syn3 and 0.9 m in Syn5. From this, it was concluded that the rate of excavation advance had little to no effect on the extent of perturbation ahead of the niche face.

### 6. Assessing damage

Damage ahead of the niche face was assessed by integrating the data and observations collected in the field with the stress analyses carried out via the numerical simulations. While field data and observations provide phenomenological evidence of

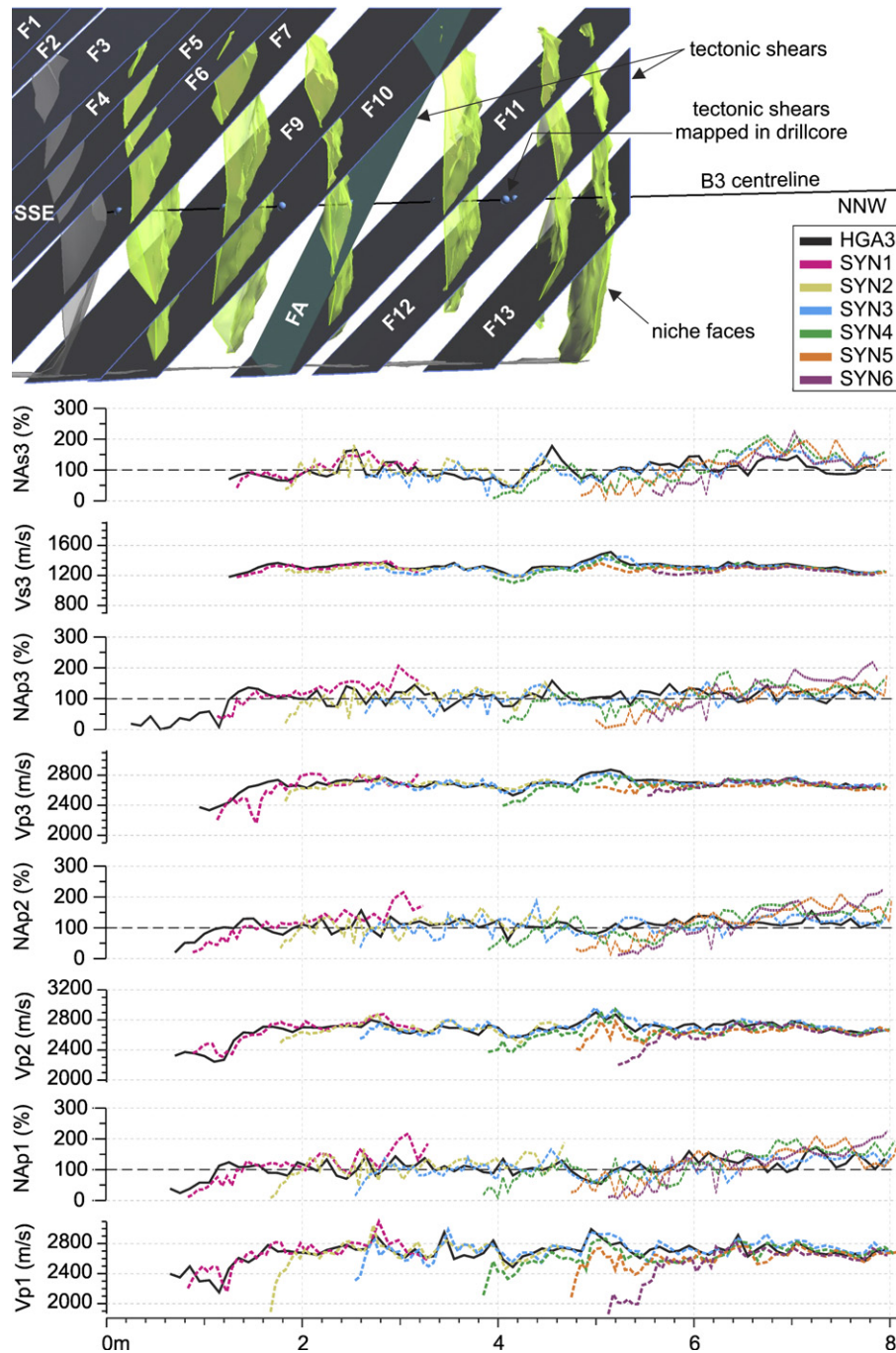


**Fig. 7.** Derived seismic parameters from all measurement campaigns taken along the east borehole wall of BEZ-B3: P-wave velocities ( $V_p$ ) and normalised amplitudes ( $NA_p$ ) for all three channels (numbers in axis labels) and S-wave velocities ( $V_s$ ) and normalised amplitudes ( $NA_s$ ) for channel 3. Benchmark measurements were made in the pre-excavation stage (HGA3). (For interpretation of references to colour in this figure, the reader is referred to the web version of this article.)

excavation-induced damage, the stress analysis provides a framework for its interpretation.

Stress-driven failure depends on the rock mass strength, the in situ stress magnitudes, and principal stress orientations. Brittle rock fails in tension by spalling at low confinement or in shear at higher confinement (Fig. 9). In tension, failure is controlled by the first crack or crack initiation. Above the damage initiation threshold and under low confinement, spalling (or extension fracturing) occurs due to the propagation and coalescence of individual cracks. In regions of high confinement, cracks interact until shear failure occurs by shearband formation.

To capture the full range of failure modes (Fig. 9), rock strength is commonly defined from laboratory testing under various deviatoric

stress states. In compression, failure involves a number of thresholds [4]: crack closure, crack initiation, crack interaction, and peak strength. When a laboratory sample is initially loaded, existing cracks close. Subsequently, the stress-strain behaviour is linear and elastic until new crack damage is initiated. At crack initiation, the onset of micro-fracturing is marked by a continuous detection of acoustic emissions beyond background levels with crack orientations parallel with the largest compressive load. Crack propagation follows with a preferred orientation in the direction of the largest compressive load. With increasing load, a critical crack density is reached when cracks interact: thus, reaching the crack interaction threshold. The interaction threshold is most commonly associated with a reversal in volumetric strain and represents the yield

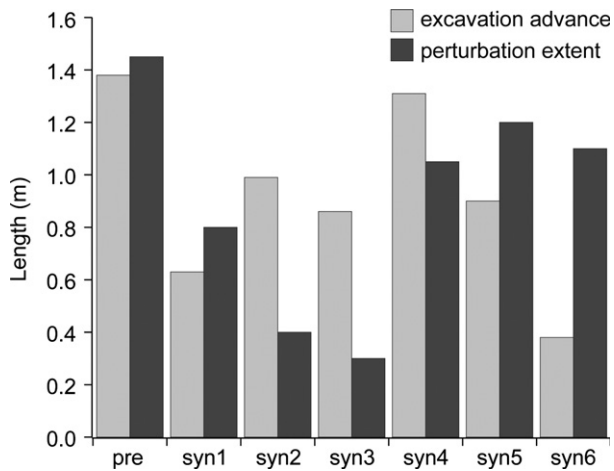


Fig. 8. EZ-B niche excavation advance and extent of induced perturbation determined from repeat seismic measurements (see Fig. 7).

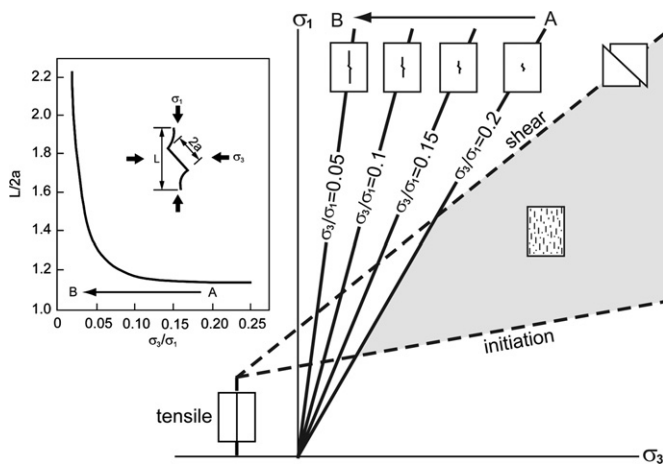


Fig. 9. Brittle failure modes compared with the length of stable crack propagation where “L” represents the total stable crack length and “2a” is the initial elliptical flaw length (modified from [25] and [23]).

(or long-term) strength [3]. Unstable crack growth continues until the sample can no longer sustain increased loading and a peak is reached (or short-term strength). Shear failure ensues.

The strength envelope (Fig. 9) is thus assembled using the thresholds described above. Crack initiation and interaction thresholds define the specific shape in regions of low confinement where the former represents the in situ lower bound strength while the latter represents the upper bound [22,23]. The transition from crack initiation to interaction (or yield) is controlled by the spalling limit (i.e.,  $\sigma_3/\sigma_1$ ), which represents a critical confinement ratio [22,23,24] when tensile failure coalescence is suppressed. Experimental studies [24,25] have shown that crack growth increases significantly once the spalling limit is below 0.05 (inset of Fig. 9): increasing crack growth implies increasing damage, which in turn infers strength reduction. Influential factors in this process include excavation damage (e.g., stress rotation), variability (e.g., scale effects), and heterogeneity (e.g., rock mass structure).

### 6.1. Defining the EZ-B strength envelope

The Mohr–Coulomb strength envelope (with cohesive strength of 3.6 MPa and frictional strength of  $25^\circ$ ) shown in Fig. 10 was obtained by averaging laboratory-determined cohesive and frictional strength components obtained from loading samples in directions that were parallel with and perpendicular to bedding

[20,21]. The spalling limits in Fig. 10 are defined based on the recent work of Amann et al. [26], which involved undrained single- and multi-stage triaxial testing of samples with loading perpendicular to bedding.

The damage initiation threshold in Fig. 10 is roughly defined based on seismic wave characteristics determined from true-triaxial tests rather than volumetric strain reversal. Popp and Salzer [27] found that volumetric strain is additionally affected by compaction perpendicular to bedding for transverse isotropic materials like the Opalinus Clay at Mont Terri. Laboratory testing showed that the onset of  $V_s$  reduction coincides with the initiation of micro-cracking as a result of localised stress concentrations whereas progressive crack opening is required to affect  $V_p$  [27]. This is attributed to a greater sensitivity of  $V_s$  to initial flat micro-cracking that results in apertures opening parallel with S-wave particle movement. In contrast, such opening direction has little effect on the corresponding P-waves propagation because particle motion is perpendicular to the direction of crack opening. At confining stresses less than 15 MPa, Zhang and Rothfuchs [28] found that volumetric strains reverse near the same stress levels as  $V_p$  reduction. Popp and Salzer [29] determined that  $V_s$  reversal occurs at roughly 60% of peak strength and  $V_p$  reversal occurs at 70%. In Fig. 10, the damage (crack) initiation threshold has been estimated based on the lower  $V_s$  reversal. The higher  $V_p$  reversal and/or volumetric strain reversal is assumed to coincide with the crack interaction threshold. Recent uniaxial compression testing (bedding-perpendicular loading) by Amann et al. [30] placed crack initiation around 30% of the rupture stress while crack damage occurred at about 70%.

### 6.2. Damage ahead of the advancing face

Evolution of the stress state ahead of the niche in response to the various nearby excavation activities was extracted from the numerical simulations and evaluated with respect to a strength envelope that was estimated based on laboratory testing (Fig. 10). Each line in Fig. 10 represents the stress state along the centreline of borehole BEZ-B3 up to 10 m from the pre-excavation borehole collar (HGA3 in Fig. 10). As BEZ-B3 is shortened, the number of points plotted decreases as excavated zones were removed in successive simulations from HGA3 onwards. Consequently, the end of each arrowhead in Fig. 10 represents a point that is 3–14 cm ahead of the advancing borehole collar. The solid circles represent the stress state about 0.5 m from the borehole collar. It should be noted that the plot for the end of the Gallery04 excavation (GA4) is equal in borehole length to that of the pre-excavation borehole length (HGA3): i.e., for both plots, the end of the arrowhead is about 11 cm and the solid circle is about 55 cm ahead of the pre-excavation borehole collar.

In general, the stress analyses (Fig. 10) illustrate that for both the isotropic (CIE) and anisotropic (or transverse isotropic in this study, CAE) cases, the minimum to maximum principal stress ratio decreases along BEZ-B3 as the near field (i.e., face of the niche) is approached from the far field (i.e., end of the borehole). This trend is already apparent once the niche entrance is excavated (HGA3) and continues in all niche excavation steps (SYN1 to SYN6). As noted earlier, no induced fractures were mapped in the BEZ-B3 drillcore ahead of the niche face in the pre-excavation stage (HGA3) despite stress ratios of less than 0.05 in the first 50 cm in both isotropic (CIE) and anisotropic (CAE) simulations (Fig. 6). However, seismic wave velocities and amplitudes are lowest in these first 50 cm (Fig. 6): suggesting that damage is evident but perhaps microscopic in scale. This is supported by the stress state of the borehole at depths greater than 0.5 m and up to about 2.3 m for CIE and 1.5 m for CAE (Fig. 10), which are above the crack initiation threshold but below the crack interaction

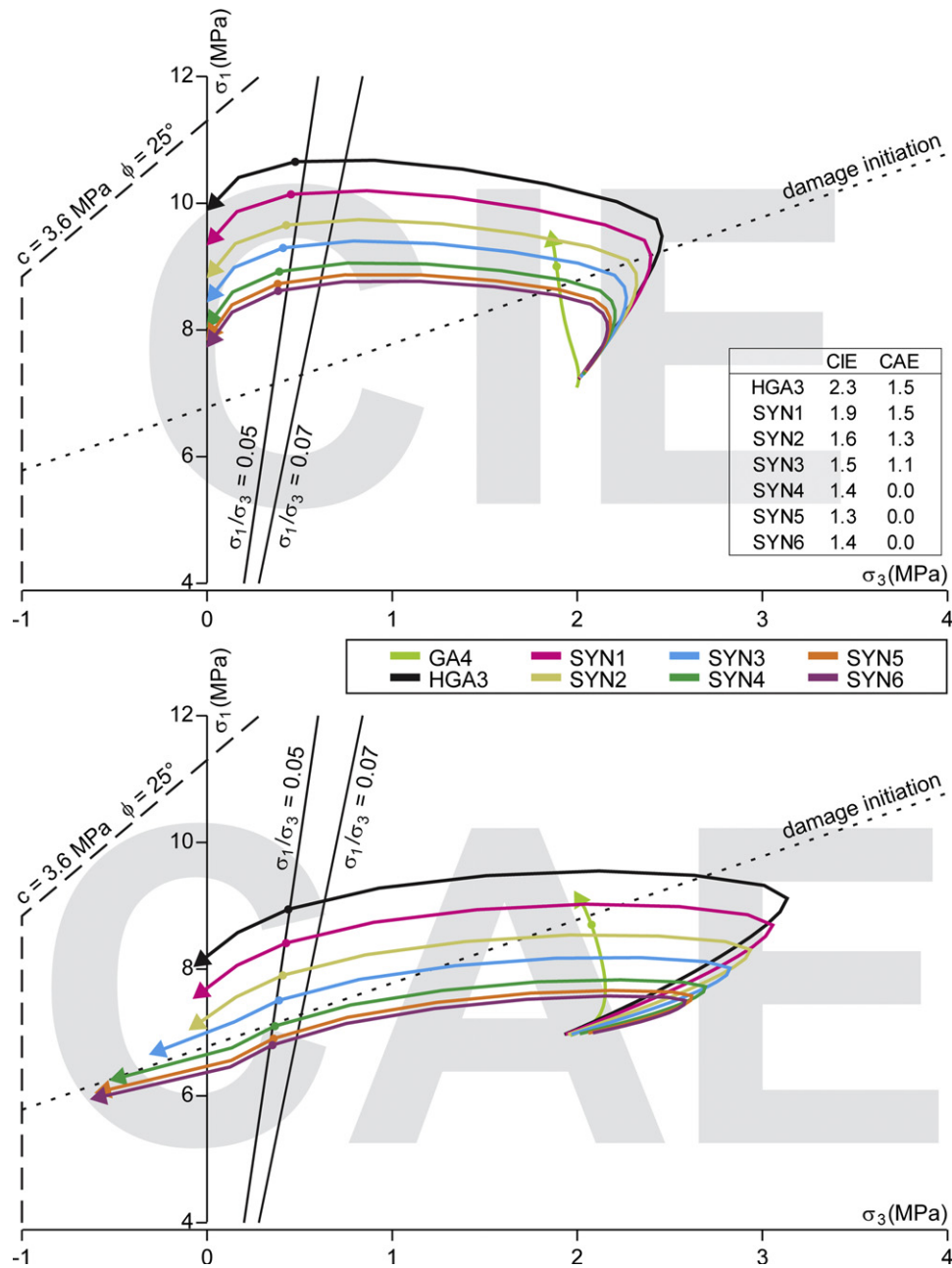


**Fig. 10.** Stress redistributions along BEZ-B3 from the isotropic model (CIE) in the top and transverse isotropic model (CAE) in the bottom. Refer to Fig. 1 for borehole location and Fig. 5 for excavation sequence. Inset of table is length of borehole (in metres) above damage initiation line, taken from advancing borehole collar. (For interpretation of references to colour in this figure, the reader is referred to the web version of this article.)

threshold. This suggests that the damage in this volume of rock most likely consists of the accumulation of propagating micro-cracks. It is important to note that this volume of rock diminishes with successive excavation advance. In the pre-excavation stage (HGA3), the volume of rock above the initiation threshold is about 2.3 m in the CIE scenario and 1.5 m in the CAE scenario. In Syn6, the volume reduces to 1.3 and 0 m the CIE and CAE cases, respectively.

Differences between the two numerical scenarios, isotropic in CIE and transversely isotropic in CAE, include the disparity in the volume of rock above the crack initiation threshold and the tensile stresses that develop near the advancing borehole collar with successive excavation (Fig. 10). This demonstrates the influence of the geological and tectonic structures; the ubiquitous and persistent nature of the bedding and bedding-parallel shears create

paths of least resistance. Tectonic shears were found to be a factor in the development of induced fractures in the niche entrance; these fractures were attributed to the unloading process due to the excavation of Gallery04 [31]. Unloading of the rock mass closest to the advancing niche face is exacerbated by the shears. Advance of the niche against the dip of these structures progressively reduced the kinematic restraint of the shears thereby increasing the likelihood that the shears deformed.

This is consistent with the difference in the volume of rock above the crack initiation threshold between the two modelling scenarios. In the CIE simulations, the volume of rock above the initiation threshold reduces from 2.3 m (as tabulated in Fig. 10) in the pre-excavation stage (HGA3) to 1.5 m in Syn3 and eventually reducing to a minimum of 1.3 m in Syn5 and Syn6. The volume of rock above the initiation threshold in the CAE simulations reduces

from 1.5 to 1.1 m in Syn3. From Syn4, none of the rock mass is above the initiation threshold in the CAE simulations. This suggests that the geological structure of the rock mass up to some point between the faces of Syn3 and Syn4 is most influential since the lower CAE stress state is more consistent with the field data. The extent of perturbation determined from the seismic wave data in the pre-excavation stage (HGA3) is roughly 1.5 m and reduces to 0.3 m in Syn3 but increases to average about 1.1 m in Syn4 to Syn6 (Fig. 8). The rock mass beyond Syn3 appears to be less influenced by the bedding and shears since the volume of rock mass above the initiation threshold in the CAE simulations is very small (i.e., 0 m ahead of the advancing niche face from Syn4) whereas 1.5 to 1.3 m ahead of the advancing niche face in the CIE simulations is above the initiation threshold. This suggests that the rock mass beyond Syn3 is likely to be more constrained kinematically (the niche face at the end of Syn3 is roughly 5.5 m from the wall of Gallery04), therefore, the anisotropic nature of the bedding and shears appears to play a diminished role in this volume.

As shown in Fig. 6, the shears can affect seismic wave velocity and amplitude in a distinct manner. In the pre-excavation stage (Fig. 6), the extent of perturbation coincided with the intersection of shear F9. Additionally, a low and relatively uniform seismic wave amplitude and velocity zone is bound by shears F7 and F9. Because F9 intersects the entrance face near the invert, the maximum stress trajectory is more inclined with the dip of the shear, thereby minimising any clamping effect. Field measurements also show that the rock mass in the lower part of the niche displaced in a direction perpendicular to bedding and/or bedding-parallel shear [17]. The influence of F7 and F9 on the perturbed extent is still clearly visible in Syn1. Likewise, the impact of F13 is visible in Syn4 and its influence continues to be seen in Syn6 with the formation of step-like structures in both velocity and amplitude profiles (Fig. 7).

In addition, comparison of the repeat seismic wave data with the pre-excavation benchmark (Fig. 7) shows that Syn1 to Syn3 deviate little from background levels except in the zone closest to the borehole collar. Conversely, Syn5 to Syn6 plots reach background levels only in the last 1.6 m. Syn4 appears to be intermediary as deviations from benchmark velocities and amplitudes are less stark. Summation of the extents of induced perturbation (Fig. 8) from Syn1 to Syn3 (i.e., roughly 0.8 m in Syn1, 0.4 m in Syn2, and 0.3 m in Syn3) approximately equals the pre-excavation extent of around 1.5 m (Fig. 8). This suggests that the zone of perturbation from the excavation of Gallery04 and/or the niche entrance extended as far as the Syn3 face or 2.5 m from the entrance face. Hence, only the rock mass ahead of the Syn3 (and possibly Syn4) face was newly disturbed in the syn-excavation stage, which is consistent with the larger extents determined from Syn4 onwards (Fig. 8) and the earlier noted reduction in the extents determined for Syn1 to Syn3.

## 7. Conclusions

Field evidence for macro-damage was limited in the EZ-B investigation but seismic wave data provided a means for identifying micro-scale damage. By integrating field and numerical data, the investigation showed that geological structures (i.e., bedding and bedding-parallel tectonic shears) were most influential near the entrance but played a lesser role as the niche deepened. Additionally, a portion of the niche is located in the perturbed zone of the intersecting Gallery04.

Damage ahead of the niche face accumulated progressively as the formerly compressed volume of rock unloaded during the excavation. Maximum to minimum principal stress ratios are

lowest where seismic wave velocities and amplitudes are lowest and hence, provide clear indication of damage related to tensile stress assisted, spalling-type failure. This was corroborated in recent laboratory studies by Amann et al. [26,30], who defined the brittle failure process of the Opalinus under low confinement and demonstrated that the volumetric behaviour in the pre-rupture stage is dependent on confining stress.

The influence of geological structures is also shown to be an important factor in the development of the damage induced ahead of the niche face. In the EZ-B niche, the tectonic shears assist in the damage process as they most easily facilitate stress relief when a tunnel is advanced against dip, such as the EZ-B niche. Lower seismic wave velocities and amplitudes near the shears suggest local relaxation of the surrounding rock mass. As the advancing niche face progressively reduced the kinematic constraint of the shears, deformation of the shears were allowed.

Results from this investigation exemplified the need to consider the rock mass heterogeneity in addition to the rock matrix anisotropy if the process of damage is to be understood when both play a role. In the case of the advancing EZ-B niche face, considerations of the shears and distance from a previously stressed volume of rock were necessary to understand both the state and extent of damage ahead of the niche face. This study demonstrates that seismic wave measurements are suitable for the characterisation of the excavation-induced damage zone in shale.

## Acknowledgements

This intensely collaborative research project was funded by the Swiss Federal Nuclear Safety Inspectorate (ENSI) and in particular, Erik Frank is thanked for day-to-day support. Seismic data was provided by Kristof Schuster with field support from Torsten Tietz, Dieter Boeddener, Friedhelm Schulte, and Wilfried Stille. Geological mapping was completed by Christophe Nussbaum, Nicolas Basdertscher, and Olivier Meier. Thorsten Schulz and Hans-Martin Zogg with field support from Frank Lemy, Corrado Fidelibus, and Jonas von Ruetten carried out the laser scans. Andy Corkum provided assistance with FLAC3D. Derek Martin is thanked for participating in numerous impromptu and invaluable discussions.

## References

- [1] Read R, Martin CD, Dzik EJ. Asymmetric borehole breakouts at the URL. In: Daemen JJK, Schultz RA, editors. Rock mechanics proceedings of the 35th U.S. symposium, Reno. Rotterdam: Balkema; 1995. p. 879–84.
- [2] Abel JF, Lee FT. Stress changes ahead of an advancing tunnel. *Int J Rock Mech Min Sci* 1973;10:673–97.
- [3] Martin CD. Seventeenth Canadian geotechnical colloquium: the effect of cohesion loss and stress path on brittle rock strength. *Can Geotech J* 1997;34:698–725.
- [4] Bieniawski ZT. Mechanism of brittle fracture of rock, parts I, II, and III. *Int J Rock Mech Min Sci* 1967;4:395–430.
- [5] Eberhardt E. Numerical modelling of three-dimensional stress rotation ahead of an advancing tunnel face. *Int J Rock Mech Min Sci* 2001;38:499–518.
- [6] Armand G, Wileveau Y, Morel J, Cruchaudet M, Rebours H. Excavation damaged zone (EDZ) in the Meute Haute Marne underground research laboratory. In: Proceedings of the 11th International Congress on Rock Mechanics, Lisbon. London: Taylor & Francis/Balkema; 2007.
- [7] Mertens J, Bastiaens W, Dehandschutter B. Characterisation of induced discontinuities in the Boom Clay around the underground excavations (URF, Mol, Belgium). *Appl Clay Sci* 2004;26:413–28.
- [8] Bossart P, Meier PM, Moeri A, Trick T, Mayor J-C. Geological and hydraulic characterisation of the excavation disturbed zone in the Opalinus Clay of the Mont Terri Rock Laboratory. *Eng Geol* 2002;66:19–38.
- [9] Martin CD, Lanyon GW. Excavation disturbed zone (EDZ) in clay shale: Mont Terri. Unpublished Mont Terri Technical Report; 2004. 207 p.
- [10] Marschall P., Trick T., Lanyon G.W., Delay J., Shao H. Hydro-mechanical evolution of damaged zones around a microtunnel in a claystone formation of the Swiss Jura mountains. In: Yale D, Holtz S, Breeds C, Ozbay U, editors.

- Proceedings of the 42nd US rock mechanics symposium. San Francisco: American Rock Mechanics Association; 2008 [CD-Rom 11].
- [11] Bath A, Gauschi A. Geological setting and sample locations. In: Pearson FJ, Arcos D, Bath A, Boisson J-Y, Fernandez AM, Gaebler H.-E., Gaucher E, Gauschi A, Griffault L, Hernan P, Waber HN, editors. Reports of the federal office for water and geology. Geology Series; 2003. p. 30–5.
- [12] Nussbaum C, Bossart P, Burrus F, Badertscher N, Meier O, Nold A. Excavation of Gallery04: general documentation, deformation measurements and geological surveys. Unpublished Mont Terri technical note; 2005. 87 p.
- [13] Nussbaum C, Bossart P, von Ruetten J, Meier O, Badertscher N. EZ-B experiment: small-scale mapping of tectonic and artificial (EDZ) fractures of the EZ-B niche. Unpublished Mont Terri technical note; 2005. 23 p.
- [14] Bossart P, Wermeille S. The stress field in the Mont Terri region data compilation. In: Heitzmann P, Tripet J-P, editors. Reports of the federal office for water and geology. Geology Series; 2003. p. 65–92.
- [15] Martin CD, Lanyon GW. Measurement of in-situ stress in weak rocks at Mont Terri Rock Laboratory, Switzerland. *Int J Rock Mech Min Sci* 2003;40:1077–88.
- [16] Yong S, Loew S, Fidelibus C, Frank E, Lemy F, Schuster K. Induced fracturing in the Opalinus Clay: an integrated field experiment. In: Leung CF, Zhou YX, editors. Rock mechanics in underground construction. Singapore: World Scientific; 2006. p. 9 [CD-Rom].
- [17] Yong S. A three-dimensional analysis of excavation-induced perturbations in the Opalinus Clay at the Mont Terri Rock Laboratory. PhD thesis, Engineering Geology. ETH Zurich, Switzerland; 2007.
- [18] Schuster K, Alheid H-J, Boeddener D. Seismic investigation of the excavation damaged zone in Opalinus Clay. *Eng Geol* 2001;61:189–97.
- [19] Itasca Consulting Group Inc. Fast Lagrangian Analysis of Continua in 3 Dimensions, version 3.0. 2005.
- [20] Bock H. RA experiment: rock mechanics analyses and synthesis: data report on rock mechanics. Unpublished Mont Terri technical report; 2001. 52 p.
- [21] Bock H. RA experiment: updated review of the rock mechanics properties of the Opalinus Clay of the Mont Terri URL based on laboratory and field testing. Unpublished Mont Terri Technical Report; 2009.
- [22] Read RS, Chandler NA, Dzik EJ. In situ strength criteria for tunnel design in highly-stressed rock masses. *Int J Rock Mech Min Sci* 1998;35:261–78.
- [23] Diederichs MS. Rock fracture and collapse under low confinement conditions. *Rock Mech Rock Eng* 2003;36:339–81.
- [24] Hoek E. Brittle failure of rock. In: Stagg KG, Zienkiewicz OC, editors. Rock mechanics in engineering practice. London: Wiley; 1968. p. 99–124.
- [25] Hoek E, Bieniawski ZT. Brittle fracture propagation in rock under compression. *Int J Fract Mech* 1965;1:137–55.
- [26] Amann F, Kaiser PK, Button EA. Experimental study of brittle behavior of clay shale in rapid triaxial compression. *Rock Mech Rock Eng* 2011;45:21–33.
- [27] Popp T, Salzer K. Anisotropy of seismic and mechanical properties of Opalinus Clay during triaxial deformation in a multi-anvil apparatus. *Phys Chem Earth* 2007;32:879–88.
- [28] Zhang C-L, Rothfuchs T. Damage and sealing of clay rocks detected by permeability measurements. *Phys Chem Earth* 2008;33:363–73.
- [29] Popp T, Salzer K. HE-D experiment: influence of bedding planes. Unpublished Mont Terri technical report; 2007. 71 p.
- [30] Amann F, Button EA, Evans KF, Gischig VS, Bluemel M. Experimental study of the brittle behavior of clay shale in rapid unconfined compression. *Rock Mech Rock Eng* 2011;44:415–30.
- [31] Yong S, Kaiser PK, Loew S. Influence of tectonic shears on tunnel-induced fracturing. *Int J Rock Mech Min Sci* 2010;47:894–907.